

EFFECT OF SIMULATED AXIAL RESIDUAL STRESS AND TRANSVERSE RESIDUAL STRESS IN WELDED P92 PIPE AND PLATES INCLUDING PLASTICITY ERROR

Vinay Kumar PAL^{1*}, Lokendra Pal SINGH²

¹Department of Mechanical Engineering, Sam Higginbottom University of Agriculture, Technology And Sciences Allahabad, 211007, U.P, India, e-mail: gaurishankar.vinaypal@gmail.com

²Department of Mechanical Engineering, Sam Higginbottom University of Agriculture, Technology And Sciences Allahabad, 211007, U.P, India

(Received 09 June 2022, Accepted 25 August 2022)

Abstract: The paper deals with the measurement of residual stresses in P92 welded pipe using the blind hole drilling technique. The post weld heat treatment (PWHT) of a P92 welded pipe was also conducted to study their effect on residual stresses. The P92 pipe weld joints were prepared using gas tungsten arc welding process. The residual stress measurement was carried out using a strain gauge rosette that was associated with the plastic deformation of the material and a stress concentration effect of a multi-point cutting tool. A corrective formulation was developed for calculating the corrected value of residual stresses from the experimentally obtained strain value. The Strain gauge response was estimated experimentally using tensile testing for uniaxial loading while a finite element analysis was performed for biaxial loading. A gas tungsten arc welds joint was prepared for a conventional V-groove and a narrow groove design.

Keywords: shrinkage stress; residual stress, v-groove; narrow groove; plasticity; PWHT

1. INTRODUCTION

Joining of the structural component, piping and pressure vessels used in nuclear, thermal fertilizer and chemical power industries are generally carried out by a welding process that results in residual stress, shrinkage stress and distortion at markable levels. In a welding process, localized heating and cooling leads to the formation of complex residual stress and distortion that results in a catastrophic failure of the welded joint. Localized heating and cooling of the base, solidification shrinkage of the weld, internal constraint, an external constraint like tacking, and phase transformation result in the formation of residual stresses and distortion [1-3]. A differential contraction of the weld and adjacent base metal causes the thermal straining that leads to distortion and shrinkage stress in welded structure [4-5]. Thermal straining along the welding direction results in the formation of longitudinal shrinkage while the strain perpendicular to the direction of welding cause the transverse shrinkage [6]. The welding distortion occurs due to the internal forces developed in the structure form the resulting

combined stresses. Distortion is treated as a pattern of permanent strains that remains in the structure after the completion of the welding process. In an arc welding process, the material is subjected to temperature more than the melting temperature of the metal. The welding cycle is elevated to rapid heating and cooling. Compared to the weld structure, the size of the weld pool is very small, and expansion and contraction of the weld is prevented by the adjacent base metal. During the heating cycle, an expansion of the heated zone leads to the formation of compressive residual stress and the cooling cycle results in shrinkage which is prevented by the base metal. After the cooling, shrinkage resistance causes the formation of tensile residual stress in the weld zone which is balanced with the compressive residual stress of the base metal [3]. Distortion and residual stress cannot be removed completely but it can be minimized. Excessive constraint during the welding process leads to the formation of high residual stress while low residual stress formed during free expansion and contraction. During the welding process, the parent metal will either resist the distortion or shrinkage

resulting in residual stress, or it follows the shrinking movement of the weld pool resulting in distortion and shrinkage [7]. The residual stress and distortion are influenced by many parameters like the welding process, welding parameters, the number of processes, groove geometry, material properties and phase transformation. Weld induced tensile residual stress in welded components leads to the HIC, buckling deformation, stress corrosion cracking (SCC), a reduction in fatigue life and brittle fracture [8–10]. Solid phase transformation and welding boundary condition play a crucial role in final stress distribution. Solid phase transformation occurs in two different manners. The first one is the formation of secondary phase particles during the heating process and the second one is the transformation of the matrix from one atomic packing to other during the heating and cooling process. Transformation occurs during the heating and the cooling cycle influences the formation of residual stress level. The character of the material is mainly responsible for the phase transformation. In P91 steel, martensitic transformation occurs during the welding cycle whose effect is more complex and acts to influence the level of stress in the transformed zone. Cottam *et al.* [2] studied the effect of both types of phase transformation on stress formation. They had reported that martensitic transformation is more complex and helps to reduce the magnitude of residual stress in the transformed zone. The point at which martensitic transformation starts results in an increase in the stress level in the adjacent non-deformed zone. In P91 steel weldment, the cooling cycle leads to the transformation of austenite to martensite. During the transformation from austenite, the stress level was observed to be decreased up to Ms temperature and after that increased to final martensitic transformation. The austenite to martensite transformation resulted in the formation of compressive stresses. The tensile residual stress was reduced with an increase in the volume fraction of martensite by controlling the heat input and the cooling rate. Austenitizing of steel results in structure transformation from BCC (ferrite) to FCC (austenite) that leads to a reduction in the volume. During the cooling process, the transformation of austenite to martensite results in a BCT structure formation that leads to an increased volume, [11]. Dong *et al.* [12] studied the effect of pipe wall thickness on residual stress distribution. Pipe wall thickness showed a strong influence on residual stress specifically on the axial component of residual stress. Axial residual stress showed a compressive nature at the outer surface while tensile at the inner surface near the vicinity of weld. An axisymmetric model was also developed for a numerical prediction of residual stress. In the start and stop points of welding, the presence of both high magnitude tensile and compressive resulted in stress gradient. Yaghi *et al.* [11] studied residual stress

distribution in a P92 welded pipe by incorporating solid phase transformation. It was observed that solid-state phase transformation (SSPT) in P92 welding has a great influence on residual stress distributions and their magnitude. Zubairuddin *et al.* [13] also reported a martensitic phase transformation effect on residual stress distribution and observed almost similar results. SSPT during welding resulted in considerable lowering in the magnitude of axial and hoop stress on the outer surface of the welded pipe (HAZ) and half of the weld fusion zone. Den and Hidekazu [14] reported that martensitic transformation not only reduced the magnitude of residual stress but also altered the sign of residual stress. The FE simulation showed a good agreement with experimental results when martensitic transformation was taken into account. Murkawa *et al.* [15] continued the same research and studied the effect of Ms temperature on the magnitude of tensile residual stress developed in the weld zone. A low Ms temperature helped to develop a compressive stress component that reduced the magnitude of net tensile residual stress within the fusion zone. The magnitude of compressive stress was observed to be increased with a decrease in the Ms-temperature and became saturate at a temperature about 200°C. The tensile nature of longitudinal stress developed in the heat affected zone was observed to be unaffected by Ms-temperature. Preheating also had a great influence on the magnitude of residual stresses and their distribution. Preheating before welding caused a considerable lowering of the peak temperature and the cooling rate. Zubairuddin *et al.* [13] reported that preheating resulted in a reduction in peak tensile residual stress and distortion. Finite element (FE) modeling is most commonly used in a numerical analysis [16-17]. A lot of work has been performed related to study the effect of the welding process, groove geometry, welding parameters, PWHT and the number of welding passes on shrinkage and shrinkage stress in a pipe and plate weldments [18], [19]. Ghosh *et al.* [6] performed an analytical study on a shrinkage stress mode, magnitude and distribution in different quadrants of GMAW and a pulse GMAW welded pipe for different weld groove designs. The mode and magnitude of shrinkage stress in different quadrants was observed to be non-uniform and varied as a function of the welding process, parameters and groove geometry. The pulse GMAW process resulted in a lower magnitude and a uniform distribution of transverse shrinkage stress compared to GMAW. A higher heat input during the welding process resulted in a higher magnitude of transverse shrinkage stress. For a constant heat input, a narrow groove design produced lower shrinkage stress compared to a conventional groove design. Multi-pass welding, the weld metal is subjected to localized solidification shrinkage [20]. A repetitive influence of the thermal cycle from subsequent weld passes affects the

development of stress in the weld groove up to a certain extent, and finally, it causes a continuous change in the groove design and the groove area with every weld pass [12]. A change in the groove size with a subsequent pass results in the groove angle variation and it will not be uniform at all locations in each quadrant of the pipe. The change in the groove size and groove area was observed to be greater in the case of a V-groove weld design than narrow-groove and this occurred due to a smaller weld metal deposition in a narrow groove. Sattari-Far and Javadi [21] studied the welding sequence effect on distortion in pipe-pipe butt joints. The experimental results were validated with a numerically obtained value. Welding leads to a diametrical variation in the pipe that mainly depends on the welding sequence. A diametrical variation in the welding section was observed to be decreased (negative) and it became zero at some distance away from the welding section and afterwards it increased. Deng *et al.* [20] performed a residual stress estimation in a multi-pass butt-welded thick pipe using a strain gauge method and the experimentally observed residual stress value matched with the numerically obtained residual stress value from a 2-D axi-symmetric FE model. The influence of weld metal yield strength on residual stress was also observed. The stresses induced in the material during the strengthening and heat treatment process as observed to have a great effect on residual stresses. The strengthening of the material resulted in a significant increase in the material's yield strength and this might be the cause of a higher residual stress after welding. Kim *et al.* [22] predicted the residual stress distribution in a P92 welded structure by using the neutron diffraction technique and to enhance the quality of results, the experimental results fairly matched with the numerical results obtained from an FE simulation. The welding sequence has a great influence on residual deformation. Ghosh *et al.* [23] studied the effect of the Pulse GMAW and GMAW process on transverse shrinkage stress and distortion of a thick butt welded plate. It was observed that the use of pulse GMAW produced low shrinkage stress, bending stress, and distortion compared to the GMAW process. For a given heat input, a narrow groove weld design produced lower stresses and distortion compared to a V-groove design but a too much narrow groove resulted in higher bending stress. For a narrow groove weld design with pulse GMAW, about 35-45% reduction in transverse shrinkage was reported compared to conventional V groove pulse GMAW and SMAW [24]. Arunkumar *et al.* [25] reported that the GTAW process minimized transverse shrinkage about 30% compared to the GMAW process due to a lower heat input application in GTAW. Basavaraju performed a simplified elastic-plastic approach to measure strains formation due to a radical shrinkage of the pipe butt weld [7]. A number of works also reported, in relation

to 3D finite element (FE), a simulation of residual stress and distortion. Yaghi *et al.* [26] performed a comparative study of a numerically and experimentally evaluated residual stress value for P92 pipe weldments and showed a good agreement between the results. The residual stresses at the outer surface were measured using X-ray diffraction while the inner surface residual stress measurement was performed using a deep-hole drilling technique. Paddea *et al.* [27] performed an experimental study to measure residual stress distribution in a P91 girth pipe weldment and also to study the effect of PWHT on their magnitude and distribution. The boundary of HAZ and the base metal (IC-HAZ) showed the maximum tensile residual stress value of about 600 MPa. The maximum tensile hydrostatic stress (400 MPa) was also observed near the vicinity of HAZ. The PWHT resulted in a considerable lowering in residual tensile stress (about 24% of yield strength of the base metal) and hydrostatic stress (50 MPa). Compressive residual stress was reported in the weld fusion zone near the final weld pass. Venkata *et al.* [28] studied the effect of PWHT on residual distribution in an electron beam welded P92 plate. Residual stress was measured using a neutron diffraction technique and compared with numerically predicted values. To minimize residual stress, the maximum PWHT duration about 2 hours and temperature about 770°C below than Ac1 temperature was reported. Chuvas *et al.* [29] also reported that PWHT at 760°C for 2 h resulted in a drastic decrease in the residual stress value both in the root and cap of the weld. Kulkarni *et al.* [30] had performed a comparative analysis of SMAW, GMAW and pulse GMAW processes and their effect on residual stress formation during welding of a thick stainless steel pipe. The pulse GMAW process produced relatively lower residual stress at the top and root of the weld. Zhao *et al.* [31] also reported a high magnitude of residual stress near the start/stop position for dissimilar multi-pass welding of a 12Cr1MoV/P92 pipe. Hempal *et al.* [32] performed a residual stress measurement in multi-pass welded ferritic-pearlitic pipes, using the X-ray diffraction technique. In the weld zone, the phase transformation was observed to have a minor influence but in HAZ a great influence was observed due to the formation of a high strength martensitic phase. At the inner surface of the weld toe, maximum tensile axial residual stress was observed which is considered as preferential sites for fatigue crack initiation. The work in the field of modeling of manufacturing processes such as a electric discharge grinding process and a high speed selective jet electrodeposition process as well as a residual stress estimation and their minimization in ultrasonic assisted turning of 4340 hardened steel has also been reported in literature [33–35].

The aim of the present research work is to deal with a study of shrinkage and residual stress in conventional

TIG and narrow TIG welds using a blind hole drilling technique. The estimate was for a straining length of 55mm, at 4 different locations of the pipe during welding V-groove and narrow-groove for same processes parameter.

2. SELECTION OF MATERIALS

2.1. Groove design and welding process parameters

The experimental setup for the pipe welding, groove design for pipes, the grooved P92 pipe, the welded P92 pipe and the welding process and the welding process parameters are discussed in Table 2. The schematic diagrams of the weld passes arrangement for V-groove and narrow-groove pipe welds are shown in Fig. 1 (a) and (b), respectively.

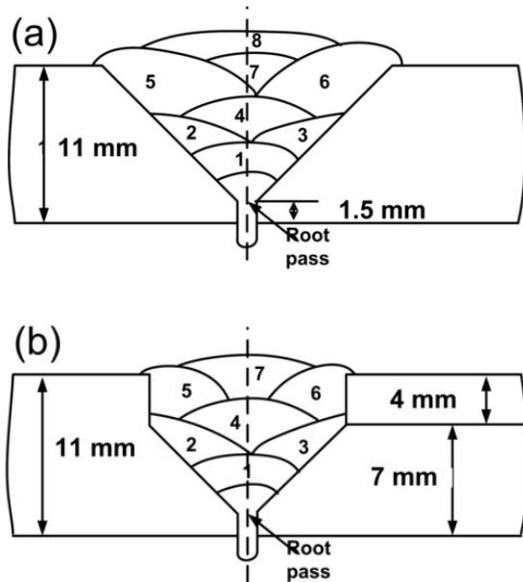


Fig. 1. Schematic diagram of weld passes: (a) V-groove and (b) narrow-groove

2.2. Measurement of shrinkage

Transverse shrinkage after each weld pass is estimated by using a digital Vernier caliper having a least count of 0.01 mm. It was estimated for a given initial straining length of 55mm at 4 different quadrants of the pipe. After each weld pass, transverse shrinkage was estimated at the some location of 4 different quadrants along the entire circumference of the pipe weld, as shown schematically in Fig. 2.

Estimation of transverse shrinkage stresses

The estimation of transverse shrinkage stress ($\sigma_{tr(i-j)}$) of a given location of pipe weld is generally considered as a function of the heat input and plate thickness. Transverse shrinkage developed during a solidification of the weld deposit in various quadrants is analyzed on the basis of variation in the groove

opening under different welding processes, procedures and parameters.

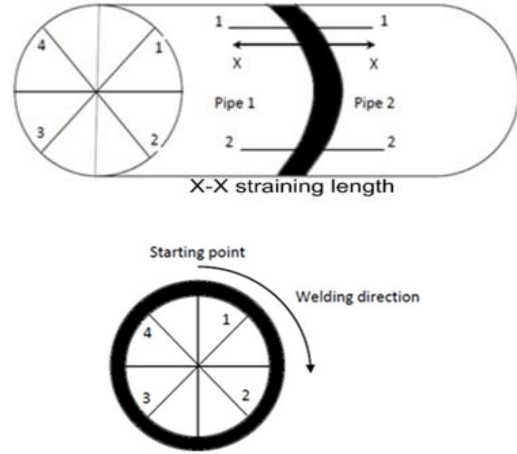


Fig. 2. Schematic diagram of the measurement of transverse shrinkage at different locations of pipe weld.

It was calculated through an evaluation of transverse shrinkage, a number of passes and an average thickness of the weld metal deposited per layer. It is given by [23];

$$\sigma_{tr(i-j)} = \frac{\Delta tr(msd)}{N} \times \frac{a}{h} \times \frac{E}{L_s}, \quad (1)$$

where: $\Delta tr(msd)$ – transverse shrinkage, mm; N – number of weld layer; E – modulus of elasticity, GPa; L_s – straining length (55 mm)(Fig. 1); h – wall thickness of the pipe, a – average thickness of weld metal deposited per layer.

After calculating transverse shrinkage stress ($\sigma_{tr(i-j)}$) at each location of the pipe weld, the average transverse shrinkage stress (σ_{avg}) generated in the entire pipe weld was divided into the four quadrants along with its standard deviation which was estimated as follows:

$$(\sigma_{avg}) = \sum_{i=0}^4 \frac{\sigma_{tr(i-j)}}{4}. \quad (2)$$

Standard deviation equal to:

$$\sqrt{\left(\frac{1}{4} \times \sum_{i=0}^4 (\sigma_{tr(i-j)} - \sigma_{avg})^2\right)}. \quad (3)$$

Based on an estimation of transverse shrinkage stress at a different location of the pipe weld, transverse shrinkage stress in each quadrant was estimated by considering the average transverse shrinkage stress at the end point of any quadrant:

$$\sigma_{(i-j)} = \frac{\sigma_{i-i} + \sigma_{j-j}}{2}. \quad (4)$$

Plasticity error and measurement of residual stress in welded pipe

To measure residual stress in pipe weldments, a blind hole drilling technique was utilized using a strain gauge rosette. A plasticity effect was also considered during the hole drilling process that might lead to local yielding of the drilled hole boundary. To study the plasticity error estimation, a P92 sample was prepared. The as-received material properties are discussed above. To study the error estimation for the residual stress measurement, the hole diameter of 2 mm was selected. The strain rosette, the drilled hole diameter and the depth are shown in Table 1.

Tab. 1. Rosette type, drilled hole diameter and depth

Material	Strain rosette	Drilled hole diameter, mm	Drilled hole depth, mm
P92 steel	FRS-2-11	Ø2.0	2.0

To estimate the plasticity error coefficient, a standard methodology opted and tensile specimens were prepared. A cobalt-based end milling cutter was utilized to make a hole at the center of the strain rosette. The strain rosette was attached to a tensile specimen possessing 2 mm drilled hole diameter as shown in Fig. 3(a).

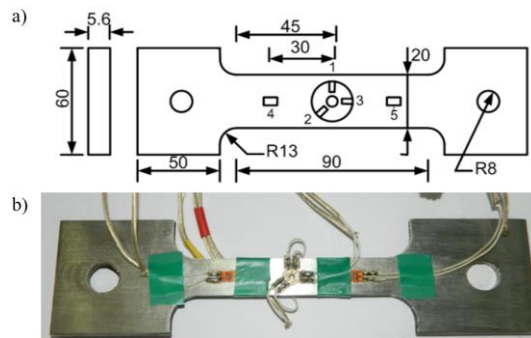


Fig. 3. Tensile specimen: (a) schematic (1, 2 & 3: strain rosette elements, 4 & 5: single element strain gauge) and (b) actual (all dimensions in mm)

Along the direction of the rosette element number 3, two single element strain gauges (4 and 5) were attached. Initially, the load was applied in various steps up to the 90% of the yield strength of P92 steel, before drilling the hole. The strains were recorded in each load step by keeping the strain gauge element 3 in the loading direction. After that, a blind hole of 2 mm diameter was made at the center of the strain rosette. After the blind hole drilling, the tensile load was applied again as per the initial process and strains were recorded. The tensile specimen used for plasticity test is shown in Fig. 3(b).

To measure residual stress in the P92 welded pipe, the blind hole drilling technique was utilized as per

ASTM E837-13a. The strain rosette is attached to the surface and make a hole at the center of strain rosette to relieve the strains. The drilling process is attributed to the stress relaxation around the hole due to the material removal. The released strains are used to calculate residual stress.

A hole of the depth of 2 mm and the diameter of 2 mm was drilled at the centre of the strain rosette by an end mill cutter and record relaxed strain using a data logger. In the P92 welded pipe, residual stresses were measured at the centre of the weld and in HAZ. The set up for the hole drilling is shown in Fig. 4. The induced plasticity error was taken into consideration in the evaluation of residual stress. The residual stresses were also measured after the PWHT of the welded pipe at 760°C for 2 h.

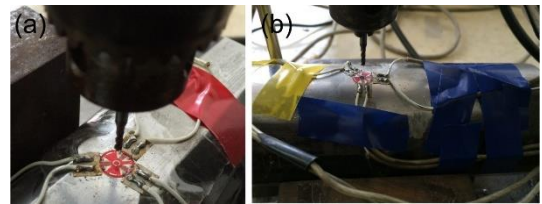


Fig. 4. Residual stress measurement setup: (a) before drilling and (b) after drilling

Measurement of residual stress in P92 welded plate

To estimate residual stresses in a P92 welded plate, cast and forged (C&F) P92 steel was selected. The microstructure, chemical composition and the mechanical properties of 'as-received' C&F P92 steel plates are discussed above. P92 weldments were produced using the shielded metal arc welding (SMAW) process for four different levels of diffusible hydrogen (as per Table 2), as discussed. The bevel angle, the root face height and the root gap were 37.5°, 1.5 mm and 1.5 mm, as shown in Fig. 5(a). The schematic diagram of the weld passes arrangement for a V-groove design is shown in Fig. 5(b). The plate dimensions and the condition of the plate before welding are discussed in (-Multi-pass welding) and plates after welding are shown in Fig. 3. The root pass was carried out using the GTAW process with AWS ER90S-B9 (9CrMoV-N) filler wire of diameter 1.6 mm for all the welds. The SMAW process was used for filling pass using a welding consumable rod of a 4 mm diameter and designated as 9CrMoV-N (AWS E9015-B9). The welding process parameters used for the GTAW root pass (top and bottom side), and SMAW filler pass are depicted in Table 2.

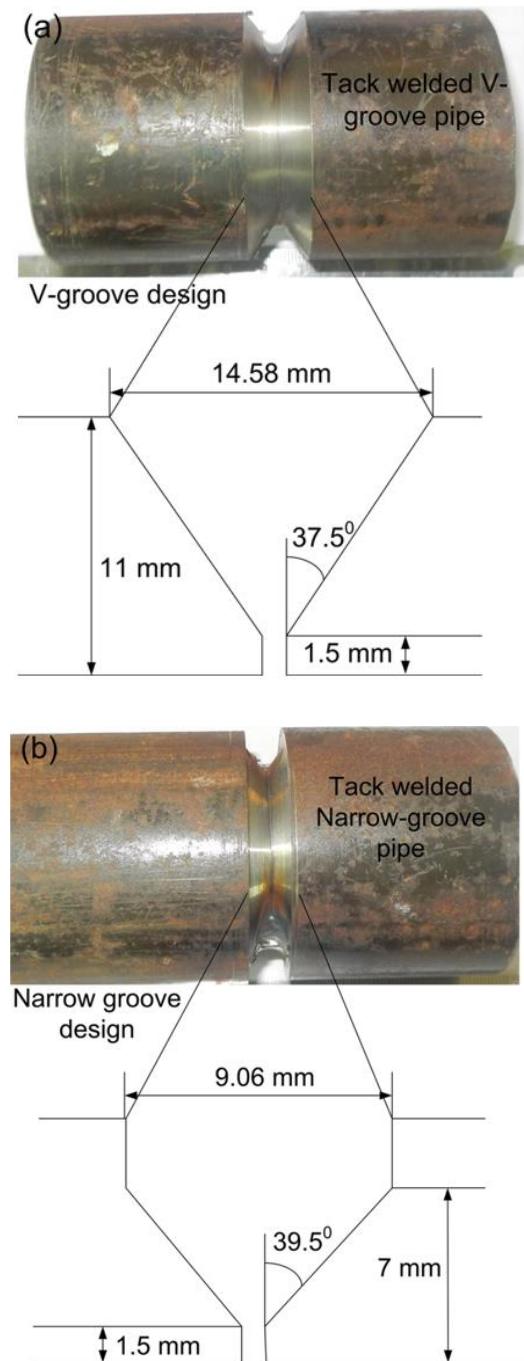


Fig. 5. (a) Schematic diagram of groove geometry and (b) weld passes arrangement (all dimensions in mm)

Tab. 2. Welding process parameters used in the welding of P92 plates

Passes	Welding process	Voltage, V	Travel speed S , mm/sec	Current, A
Root pass (1,2)	GTAW	12-16	2.14	110-120
Filling passes	SMAW	21-25.6	3.20-5.36	140-151

In a P92 welded plate, residual stresses were determined using the blind hole drilling method. In this method, relieving strains are measured using a strain gauge rosette that is attached to the specimen's surface to make a blind hole at the center of it. Principle stresses and their directions are mainly related to relieved strains. For measuring welding residual stresses, the procedure of blind hole drilling is described in literature (ASTM E837-13a).

2.3. Numerical simulation procedure

A thermo-mechanical finite element (FE) analysis conducted for the present problem utilized the temperature dependent material properties of the weld and base metal [37]. To perform an FE analysis, a rate independent thermo-elasto-plastic material and a large displacement model were utilized. The FE analysis was performed in two steps. Initially, transient temperature distribution was estimated using a thermal analysis. After the transient thermal analysis, a non-linear structure analysis was performed to predict residual stresses distribution in the welded plate.

2.4. FE model and material properties

2-D axisymmetric finite element (FE) models were developed to predict residual stress in a conventional V-groove welded plate, as shown in Fig. 6. To accommodate the steep temperature rise in the weld, fine meshing was carried out in the weld and the adjacent area of the weld as compared to the remaining part of the FE model.

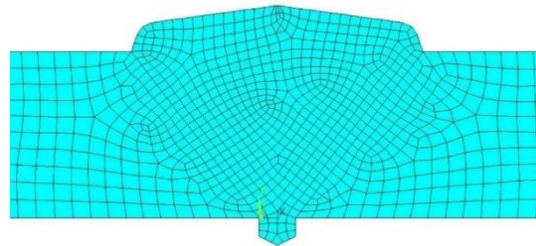


Fig. 6. 2-D meshed models for conventional V-groove design

In the E model, each pass consisted of several numbers of elements at which a heat flux was applied as per the welding pass sequence. The temperature dependent thermo-physical properties of the filler and base metal as shown in Fig. 7 are utilized for an FE simulation [26]. A comparative study was performed to study the location of a fusion boundary from the weld centerline in actual weld cross section and 2-D FE model. Five different locations were selected from the plate's inner and outer surfaces and the results are depicted in Table 3.

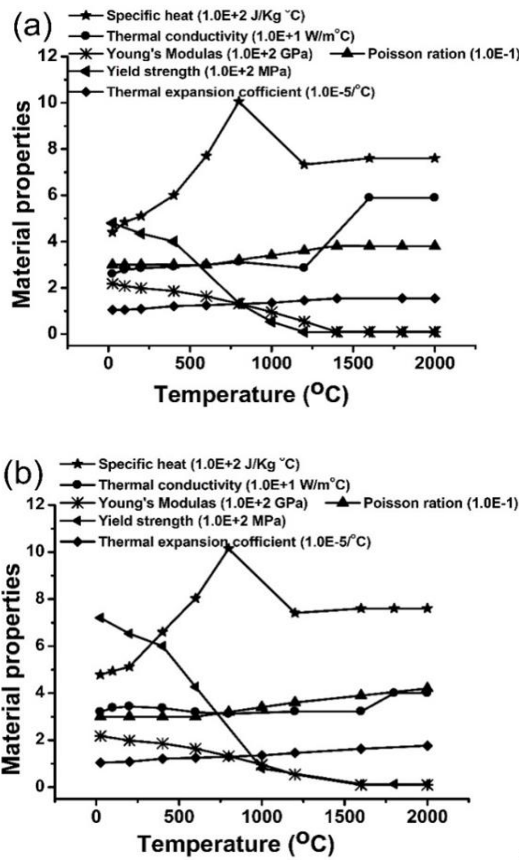


Fig. 7. Temperature dependent material properties: (a) base metal (P92 steel) and (b) weld metal

2.5. Thermal analysis

A transient thermal and non-linear structure analysis was performed to determine residual stress in the P92 welded plate. In multi-pass welding, the heating and cooling cycles were divided into several steps. FE solver ANSYS was utilized to perform a transient thermal analysis and a non-linear structural analysis for each load step of heating and cooling cycle. For the non-linear structure analysis, a transient temperature analysis was utilized as the input parameters. The heat flux was assumed to be distributed with Gaussian in nature.

An electrode feed rate and heat input during the welding processes are utilized in the determination of the size of passes in the FE model. In the welding process, primarily heat loss occurs as convection and radiation. The combined effect of radiation and convection was estimated using Eq. 5 [38], [39]:

$$h_c = 24.1 X 10^{-4} \epsilon T^{1.61}. \quad (5)$$

The element birth technique was applied to simulate each pass of the weld. Each pass was activated at a particular time at which molten metal is deposited. A similar observation was also stated by Brickstad and Josefson [40]. The heat flux calculation was done as per the literature for a set of weld parameters until a reasonable molten zone size (1340-1390°C) was obtained along the weld groove edges. The boundary at which temperature was experienced in the range of 850–950°C are considered as the heat affected zone. In multi-pass welding, the weld pass was not allowed to cool up to ambient temperature. The inter-pass temperature maintained in the temperature range of 250-300°C. Hence, for the subsequent passes, initial temperature may not be ambient temperature. The softening temperature resulted in a minute effect on the final results of the modeling. Liu et al. [41] used softening temperature of 1200°C for multi-pass steel pipe welds.

2.6. Structural analysis

A heat transfer analysis was carried out first to evaluate the nodal temperature as a function of time and compare it with experimental results. A stress-strain evaluation used in the structural analysis was expressed by [42]–[44]:

$$\{\sigma\} = [D]\{\epsilon^e\}, \quad (6)$$

where:

$$\{\epsilon^e\} = \{\epsilon\} - \{\epsilon^t\}, \quad (7)$$

$$\{\epsilon^t\} = \Delta T [\alpha_x \alpha_y \alpha_z 0 0 0]^T, \quad (8)$$

where: $\Delta T = T_n - T_\infty$ and T_n is the instant temperature at the point of interest.

Tab. 3. Comparison of fusion boundary

Points	Distance from weld root to weld top, mm	Conventional groove fusion boundary	
		From weld cross section center, mm	In FEM Model weld cross section center, mm
A	0	2.2	2
B	5	3.20	4.18
C	10	7.15	8.90
D	15	12.40	14.89
E	18	14.50	15.60

In the case of nonlinear materials, the total strain can be written as:

$$\{\varepsilon\} = \{\varepsilon^e\} + \{\varepsilon^t\} + \{\varepsilon^p\}, \quad (9)$$

where in this equation, the component on the right-hand side is of elastic strain, thermal strain, and plastic strain.

3. RESULTS AND DISCUSSION

3.1. Blind hole drilling technique

Transverse shrinkage $\Delta_{tr(msd)}$ was estimated for straining length of 55 mm, at 4 different locations of the pipe during welding a V-groove and a narrow-groove for same processes parameter. The value of shrinkage obtained during welding for a different groove design is given in Table 4. In consideration of $\Delta_{tr(msd)}$, the process of estimation of $\sigma_{w(i-i)}$, σ_{avg} and $\sigma_{(i-j)}$ for

a straining length of 55 mm is typically shown in Table 5 for sample 1 (V-groove). The estimated transverse shrinkage stresses for conventional the V-groove and the narrow-groove design are given in Table 5. Table 5 shows a wide variation in shrinkage stresses for different groove designs.

Transverse shrinkage stress and their nature for the V-groove, developed during welding are given in Table 7, 8, and 9 for samples 1, 2 and 3, respectively, for the training length of 55 mm and the heat input of 0. kJ/mm. Table 7 shows that for sample 1 of the V-groove, transverse shrinkage stresses present in the quadrants of 1-2, 4-1 are of tensile and in quadrants of 2-3, 3-4 are of the compressive mode. The average transverse shrinkage stress for the three samples is estimated at about 164.33 MPa.

Tab. 4. Measured transverse shrinkage at various locations of P92 pipe weld for different groove designs and the same welding condition for straining length of 55 mm

Sample	Type of weld groove	No. of weld layer	Heat input, kJ/mm	Estimated transverse shrinkage at various location of P92 pipe weld, mm			
				1-1	2-2	3-3	4-4
1	Conventional V-groove	8	0.47	2.24	2.11	2.34	2.20
2				2.41	2.01	2.50	2.64
3				2.52	2.29	2.86	2.41
4	Narrow V-groove	7, 8	0.47	1.47	1.52	1.63	1.38
5				1.68	1.55	1.89	1.80
6				1.52	1.37	1.49	1.49

Tab. 5. Estimation of $\sigma_{(i-i)}$ and $\sigma_{(i-j)}$ for V-groove pipe weld prepared by GTAW process

Estimation of the $\sigma_{(i-i)}$		Estimation of the $\sigma_{(i-j)}$	
$\sigma_{(1-1)} = \frac{2.24}{8} \times \frac{1.64}{11} \times \frac{210 \times 10^3}{55} = 159.39$		$\sigma_{(1-2)} = \frac{\sigma_{(1-1)} + \sigma_{(2-2)}}{2} = \frac{159.39 + 152.88}{2} = 156.13$	
$\sigma_{(2-2)} = \frac{2.11}{8} \times \frac{1.67}{11} \times \frac{210 \times 10^3}{55} = 152.88$		$\sigma_{(2-3)} = \frac{\sigma_{(2-2)} + \sigma_{(3-3)}}{2} = \frac{152.88 + 140.11}{2} = 146.49$	
$\sigma_{(3-3)} = \frac{2.34}{8} \times \frac{1.38}{11} \times \frac{210 \times 10^3}{55} = 140.11$		$\sigma_{(3-4)} = \frac{\sigma_{(3-3)} + \sigma_{(4-4)}}{2} = \frac{140.11 + 171.81}{2} = 155.96$	
$\sigma_{(4-4)} = \frac{2.20}{8} \times \frac{1.80}{11} \times \frac{210 \times 10^3}{55} = 171.81$		$\sigma_{(4-1)} = \frac{\sigma_{(4-4)} + \sigma_{(1-1)}}{2} = \frac{171.81 + 159.39}{2} = 165.60$	
Estimation of $\sigma_{avg} = \left(\frac{159.39 + 152.88 + 140.11 + 171.81}{4} \right) = 156.04$			
Estimation of S.D. = $\sqrt{\left(\frac{1}{4} \times ((156.04 - 159.39)^2 + (156.04 - 152.88)^2 + (156.04 - 140.11)^2 + (156.04 - 171.81)^2 \right)} = \pm 11.45$			

Tab. 6. Measured transverse shrinkage stress at various locations of P92 pipe welds under different groove designs and the same welding condition for 55 mm straining length

Sample	Type of weld groove	Heat input, kJ/mm	Estimated transverse shrinkage at various location of P92 pipe weld, mm				Avg+Std. Dev.
			159.39	152.88	140.1099	171.81	
1	Conventional	0.47	172.53	161.33	186.57	168.38	172.21±9.21
2			158.54	160.96	177.45	164.16	165.27±7.30
3	V-groove		89.65	112.30	111.54	119.75	108.31±11.24
4	Narrow		125.37	107.60	123.00	113.24	117.30±7.21
5			V-groove	107.49	93.91	109.25	110.54
6			159.39	152.88	140.1099	171.81	156.04±11.44

Transverse shrinkage stress in narrow groove GTA welds

The variation of the nature and magnitude of transverse shrinkage stresses at a different location of a GTA welded narrow-groove pipe for a heat input of 0.47 kJ/mm are given in Tables 10, 11 and 12 for sample 4, 5 and 6, respectively. Table 10 reveals that the nature of transverse shrinkage stresses for sample 4 present in quadrants 3-4, 4-1 are of tensile and in quadrants of 1-2, 2-3 are of the compressive mode. The average transverse shrinkage stress for the three samples is estimated at 110.30 MPa. Hence, a drastic decrease was observed in shrinkage stress for the narrow groove weld design, i.e. from 164.33 MPa to 110.33 MPa. The shrinkage stress estimated for the V-groove design was approximately 34% of the yield strength of the material and in the narrow-groove, 23% of the yield strength of the material. Hence, it can be concluded that the weld is safe from transverse shrinkage stress.

Effect of the number of passes on shrinkage

The variation in transverse shrinkage after each pass both for the conventional V-groove and the narrow-groove weld design is shown in Fig. 8. From Fig. 8, it was observed that after each pass shrinkage will increase for both groove designs, i.e., an increase in shrinkage stress. From Fig. 8, it is clear that transverse shrinkage measured in the narrow-groove is much smaller than for the conventional V-groove design.

Evaluation of coefficients from uniaxial tensile test

The magnitude and orientation of principle residual stress can be estimated using Eq. 10–12, as shown below [45].

Tab. 7. Distribution of transverse shrinkage stress at different quadrants of pipe weld prepared by using GTAW and V- groove (sample 1)

Weld location	Transverse shrinkage stress, MPa	Nature	Avg. Transverse shrinkage stress +Std. Dev.
1-2	156.13	Tensile	156.04±6.75
2-3	146.49	Compressive	
3-4	155.96	Compressive	
4-1	165.60	Tensile	

Tab. 8. Distribution of transverse shrinkage stress at different quadrants of pipe weld prepared by using GTAW and V- groove (sample 2)

Weld location	Transverse shrinkage stress, MPa	Nature	Avg. Transverse shrinkage stress +Std. Dev.
1-2	166.93	Compressive	172.20±3.92
2-3	173.95	Tensile	
3-4	177.47	Tensile	
4-1	170.45	Compressive	

Tab. 9. Distribution of transverse shrinkage stress at different quadrants of pipe weld prepared by using GTAW and V- groove (sample 3)

Weld location	Transverse shrinkage stress, MPa	Nature	Avg. Transverse shrinkage stress +Std. Dev.
1-2	159.75	Compressive	164.77±5.25
2-3	169.20	Tensile	
3-4	170.80	Tensile	
4-1	159.35	Compressive	

$$\sigma_{max} = \frac{\varepsilon_1 + \varepsilon_3}{4\bar{A}} + \frac{1}{4\bar{B}} \sqrt{(\varepsilon_3 - \varepsilon_1)^2 + (\varepsilon_3 + \varepsilon_1 - 2\varepsilon_2)^2} \quad (10)$$

$$\sigma_{min} = \frac{\varepsilon_1 + \varepsilon_3}{4\bar{A}} - \frac{1}{4\bar{B}} \sqrt{(\varepsilon_3 - \varepsilon_1)^2 + (\varepsilon_3 + \varepsilon_1 - 2\varepsilon_2)^2} \quad (11)$$

$$\tan 2\alpha = \frac{\varepsilon_3 + \varepsilon_1 - 2\varepsilon_2}{\varepsilon_3 - \varepsilon_1} \quad (12)$$

where ε_1 , ε_2 and ε_3 are the strains readings of strain rosette elements 1, 2 and 3 respectively. σ_{max} and σ_{min} are the maximum and minimum principal stresses and angle α is the angle between minimum principal stress and element 1.

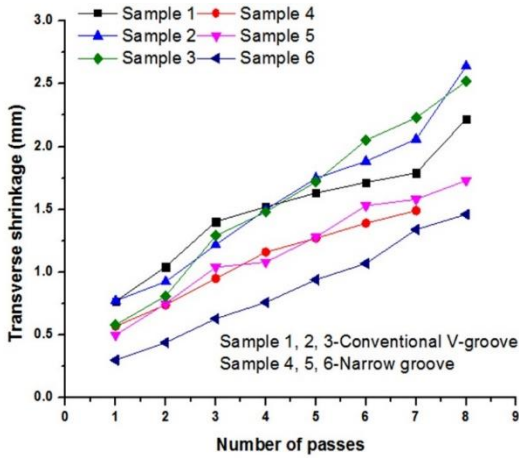


Fig. 8. Cumulative shrinkage in conventional TIG and narrow TIG welds (samples 1, 2, 3: conventional V-groove and samples 4, 5, 6: narrow groove)

In Eqs. 10 and 11, calibration coefficients \bar{A} and \bar{B} stated are calculated using Eqs. 13 and 14 [45], where $\varepsilon_{3\text{ cal}}$ and $\varepsilon_{1\text{ cal}}$ are the differences in the strain readings in directions 3 and 1, respectively, obtained from tensile testing with and without the hole in the strain rosette in the tensile testing. The variations of coefficients \bar{A} and \bar{B} with respect to the ratio of applied stress to the yield strength of the work materials are depicted in Fig. 9(a). Calibration coefficients a and b used in the calculation of residual stress measurement according to the blind hole drilling technique were also calculated according to Eqs. 13 & 14. [45]. The average values of calibration coefficients \bar{A} and \bar{B} are presented in Table 13.

$$\bar{A} = (\varepsilon_{3\text{ cal}} + \varepsilon_{1\text{ cal}})/2\sigma_{app} \quad (13)$$

$$\bar{B} = (\varepsilon_{3\text{ cal}} - \varepsilon_{1\text{ cal}})/2\sigma_{app} \quad (14)$$

$$\bar{A} = -\frac{(1+\nu)a}{2E} \quad (15)$$

$$\bar{B} = -\frac{b}{2E} \quad (16)$$

Tab. 10. Distribution of transverse shrinkage stress at different quadrants of pipe weld prepared by using GTAW and V- groove (sample 4)

Weld location	Transverse shrinkage stress, MPa	Nature	Avg. Transverse shrinkage stress +Std. Dev.
1-2	100.97	Compressive	108.30±5.78
2-3	111.92	Compressive	
3-4	115.64	Tensile	
4-1	104.70	Tensile	

Tab. 11. Distribution of transverse shrinkage stress at different quadrants of pipe weld prepared by using GTAW and V- groove (sample 5)

Weld location	Transverse shrinkage stress, MPa	Nature	Avg. Transverse shrinkage stress +Std. Dev.
1-2	116.48	Compressive	117.30±1.52
2-3	115.30	Compressive	
3-4	118.12	Tensile	
4-1	119.30	Tensile	

Tab. 12. Distribution of transverse shrinkage stress at different quadrants of pipe weld prepared by using GTAW and V- groove (sample 6)

Weld location	Transverse shrinkage stress, MPa	Nature	Avg. Transverse shrinkage stress +Std. Dev.
1-2	100.7	Compressive	105.30±4.183
2-3	101.58	Compressive	
3-4	109.90	Tensile	
4-1	109.02	Tensile	

To calculate the applied stress as per *ASTM E837-13a*, strains reading (ε_1 , ε_2 & ε_3) obtained from the strain rosette were utilized while the single element strain gauge was used to calculate the applied stress away from the hole but within the gauge length.

Eq. 16 is used to estimate the error in the uniaxial loading direction.

$$\text{Error (\%)} = 100 * (\sigma_{ASTM} - \sigma_{app})/\sigma_{app} \quad (16)$$

where σ_{ASTM} is the stress calculated from (ASTM E837-13a) as per the strain readings of the strain rosette.

Tab. 13. Calibration coefficients

Material	\bar{A} ($\times 10^{-13}$)	\bar{B} ($\times 10^{-13}$)	A	b
P91 steel	-4.58	-11.12	0.17	0.48

The error variation with respect to the ratio of the applied stress and the yield strength of the work materials (σ_{app}/σ_y) is presented in Fig. 9. The induced error was observed to increase with an increase in the ratio of the applied stress to the yield strength of the material. Hence, it can be stated that in uniaxial loading, the error value increases with higher applied stress. The error was measured in the range of 3 to 44 percent.

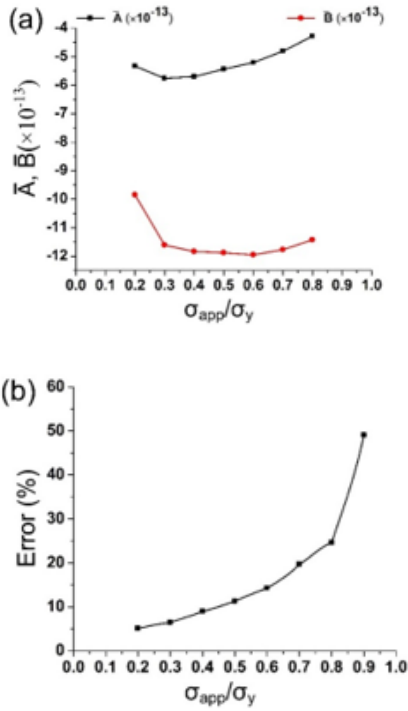


Fig. 9. Variation of calibration coefficients \bar{A} and \bar{B} (a) and percentage error vs. applied stress ratio (b)

Error estimation for biaxial stress analysis

It was observed that the % error value increased with an increase in the applied stress. The value obtained for uniaxial loading might not be used for multiaxial loading. In P92 steel, the higher yield strength of the material might lead to high residual stress. The exact magnitude of plastic yielding around the hole is very difficult to ascertain. The biaxial state of the stress applied on the strain rosette is investigated using numerical modeling. A 3-D numerical model was developed to establish the biaxial loading effect on the strain gauge rosette. Fig. 10 shows the model and meshing for the blind hole. The 3-D model was built using ANSYS and meshing was done by selecting the 8 node SOLID 185 element structural stress analysis. A 3-D FE model with dimensions 20 mm × 20 mm × 5.6 mm was prepared for 2 mm blind hole geometry. For 2 mm blind hole geometry, the elements and the nodes were 67012 and 35024, respectively.

Initially, a 2 mm hole was made and applied uniaxial loading as per experiments. As per experiments, for the numerical model, the applied load value was increased gradually along the sample axis. The response of the nodes that fall under the area of the strain rosette elements was measured to estimate the average strain value. The estimated average strain value obtained from the experiments was compared with the uniaxial experimental strain value. The strain value obtained from the uniaxial tensile tests and from the finite element modeling showed a good agreement as given in Table 14. In a biaxial stress analysis, stresses were applied in both directions and four stress ratios (SR), transverse to longitudinal stress ($\sigma_{Tapp}/\sigma_{Lapp} = 0.2, 0.6, 0.8 \& 1$) were used. For each stress ratio, the applied longitudinal stress (σ_{Lapp}) varied from 0.5 σ_y to σ_y . The strain data obtained from the model for the biaxial loading was then utilized to develop correlations for the calculation of residual stress error estimations for a strain gauge rosette having 2 mm hole diameters for P92 steel.

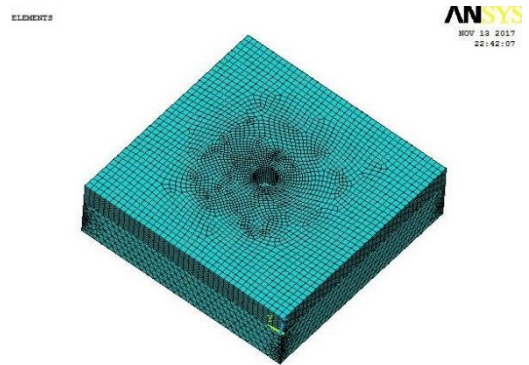


Fig. 10. Meshed model for the estimation of error in uniaxial and biaxial loading

In the blind hole drilling method, the three element strain rosette used for the strain calculation is shown in Fig. 11. The strain values ($\epsilon_1, \epsilon_2 \& \epsilon_3$) were calculated from the FE model by taking the average of the strain value at each node under the area of gauge elements, as shown in Fig. 11.

Tab. 14. Comparison of strain values (in microns)

Material	Experimental		Predicted	
	ϵ_1	ϵ_3	ϵ_1	ϵ_3
P92 steel (2 mm hole diameter)	-267	745	-247	720

The strains value were utilized to calculate longitudinal and transverse stress (σ_{Lastm} & σ_{Tastm}) based on ASTM E837-13. The percentage error of stresses in longitudinal and transverse directions are calculated using Eqs. 17 and 18, respectively.

$$\text{Error (\%)} = 100 * (\sigma_{Lastm} - \sigma_{Lapp})/\sigma_{Lapp} \quad (17)$$

$$\text{Error (\%)} = 100 * (\sigma_{Tastm} - \sigma_{Tapp}) / \sigma_{Tapp} \cdot (18)$$

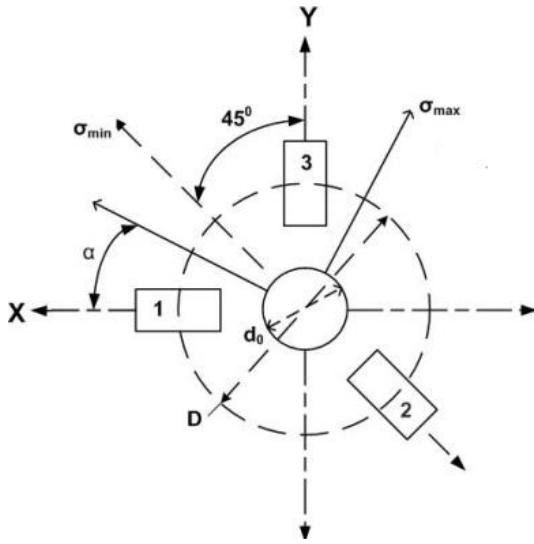


Fig. 11. Schematic of three element strain gauge rosette

Fig. 12 shows percentage errors for longitudinal and transverse directions. The transverse error observed for the stress ratio of 0.2 was much higher than the other error values calculated for another stress ratio. It was observed that for applied biaxial stress close to the yield strength of the material, longitudinal and transverse errors were the lowest, as shown in Fig. 12(a). Fig. 12(b) shows the measurement of the error in the axial and transverse direction for biaxial loading. In X-axial load is applied in a fraction of the yield strength of the material. As the applied load approaches the yield strength of the material, the error in the longitudinal direction tends to decrease while in transverse direction, it tends to increase or it remains almost constant. Further, if the load applied in both directions is be same, an error will also be high in both axial and transverse directions. When the load applied in the transverse direction decreases as compared to the axial direction, the error will also decrease both in axial and transverse directions.

In order to make the relationship between the corrected stress value and the ASTM calculated residual stresses value, a regression analysis was performed using the MINITAB software. An analysis of variance (ANOVA) was used to build the relations between the control factor and the responses. Table 15 depicts the result of ANOVA. The coefficient of determination R^2 , the proportion of variability in the data sample is 98.5 % as indicated in Table 15. The coefficient of determination indicates the adequacy of the regression Equations 11 and 12 to approximate the trend of the data sample. The adjusted R^2 is a measure of the proportion of variation in the dependent variable. Table 15 also indicates the sequential sum of square (Seq SS), the adjusted sum of square (Adj SS) and the

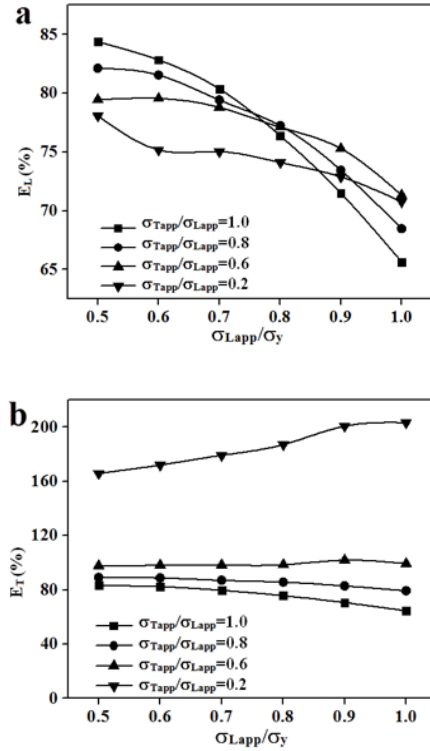


Fig. 12. Percentage error (a) longitudinal and (b) transverse for 2 mm hole

adjusted mean square (Adj MS). The adjusted sum of squares, calculated by MINITAB, is determined by an addition of each particular term to a regression model considering the effect of other terms also found in the model. The ANOVA is used to investigate the significance of factors and their interaction with the responses. The mean square (MS) MS in the ANOVA table is calculated as below:

$$MS = \frac{SS(\text{Sum of square deviation})}{DF(\text{Degree of freedom})} \cdot (19)$$

The degree of freedom, the F value, is indicated as below:

$$F = \frac{MS \text{ for a term}}{MS \text{ for the error term}} \cdot (20)$$

The probability of significance (P value) is then calculated based on the F value. If the probability of significance (P value) is less than 0.05, then it can be stated that the effect of the control factors is significant in the regression relations.

The ratios of the ASTM calculated stresses to yield strength (σ_{rastm}/σ_y and σ_{lastm}/σ_y) were also utilized to develop the relationship between the ASTM calculated and corrected residual stress values. Equations 21 and 22 show the relations. An analysis of variance for P92 steel of a 2 mm hole diameter is shown in Table 15. The error in the residual stress calculation depends on factors like biaxial stress ratio, the yield strength of the material, and stress applied.

$$\sigma_L = -32.7 - 241 \frac{\sigma_{Lastm}}{\sigma_y} - 0.006 \sigma_{Tastm} + 1.2 \sigma_{Lastm} \tag{21}$$

$$\sigma_T = -6.21 + 404.58 \frac{\sigma_{Tastm}}{\sigma_y} - 0.26 \sigma_{Tastm} - 0.109 \sigma_{Lastm} \tag{22}$$

3.2. Residual stress estimation in P92 welded pipe

The axial and hoop stress results are depicted in Table 16. At the center of the weld fusion zone, the predicted nature of axial and hoop stress was tensile stress. The maximum predicted hoop stress in the weld zone was about 226±15 MPa in the V-groove weld design while the minimum was about 108±5 MPa in the narrow groove design. The maximum and minimum predicted axial stresses were 220±12 MPa and 148±17 MPa for the V-groove and narrow-groove designs, respectively. At the center of the heat affected zone (HAZ) (approximately 8 mm for V-groove and 7 mm for narrow groove design), the magnitude of residual stresses was observed to be tensile in nature

with a lower magnitude as compared to the weld fusion zone. In the V-groove design, the magnitude of axial and hoop stresses was 137.98 MPa and 104.69 MPa, respectively, while in the narrow groove design, the magnitude was 100 and 92.93 MPa, respectively. The corrected residual stresses values were calculated using Equations 21 and 22. The yield strength of the material was considered to be 450 MPa. The maximum corrected axial residual stress value (112±8 MPa) was obtained for the V-groove design, which was 30.66 % of the yield strength of the material. The corrected residual stresses value obtained for the V-groove and narrow-groove designs were too much low as compared to yield strength of the material.

After the post weld heat treatment of 760°C for 2 hrs., there was a considerable lowering in the magnitude of residual stress without affecting its nature, as given in Table 16. At the weld center, the maximum hoop and axial stresses were measured to be 105 MPa and 85 MPa respectively, for the V-groove design. For the narrow groove design, hoop and axial stresses were measured

Tab. 15. ANOVA Table of σL and σT for modified Cr-Mo alloy (2 mm hole)

Analysis of Variance for σ _L : (Response Surface Regr: R-Sq = 98.5% R-Sq(adj) =98.4%)						
Source	DF	Seq SS	Adj SS	Adj MS	F	P
Regression	3	125750	125750	41916.8	1219.14	0
Linear	3	125750	125750	41916.8	1219.14	0
Residual Error	20	687	687	34.4		
Total	23	126437				

Analysis of Variance for σ _T : (Response Surface Regr: R-Sq =99.4% R-Sq(adj) = 99.3%)						
Source	DF	Seq SS	Adj SS	Adj MS	F	P
Regression	3	276248	276248	92082.7	1152.27	0
Linear	3	276248	276248	92082.7	1152.27	0
Residual Error	20	1598	1598	79.9		
Total	23	277846				

Tab. 16. Results of residual stresses

Welding condition	Groove design	Center of the weld				Center od HAZ			
		ASTM value of residual stress		Corrected residual stress		ASTM value of residual stress		Corrected residual stress	
		σ _T	σ _L	σ _T	σ _L	σ _T	σ _L	σ _T	σ _L
As welded	V-groove	226±15	220±12	114±10	112±8	104.69	137.98	28.54	71.79
	Narrow groove	108±5	148±17	45±2	65±11	92.93	100.02	27.09	42.94
PWHT	V-groove	105	85	52	23	49	54	19	4
	Narrow groove	57	73	23	15	51	54	20	3

to be 57 MPa and 73 MPa, respectively, which was approximately half of the previous value (the as-welded condition). In HAZ, axial stress was observed to be only 0.66% of the yield strength of the material. During the welding process, a smaller volume of the weld metal was deposited in the narrow-groove weld as compared to the V-groove weld and it might be the reason for a lower magnitude of residual stresses in the narrow groove weld design as compared to the V-groove weld design. A lower volume of the metal deposited provides a lower resistance to shrinkage and hence the magnitude of residual stresses is lower in the narrow groove weld.

Residual stress estimation using experimental method

In the blind hole drilling method, the stress concentration factor and plasticity lead to an overestimation of the strain data. To overcome the effect of stress concentration and plasticity during the residual stress measurement, the induced error was estimated for the strain gauge FRS-2-11 after drilling a hole of a 2 mm diameter, as given in Equations 21 and 22. The residual stress for the different conditions of the welded plate is presented in Table 17. The effect of the diffusible hydrogen content on residual stress distribution did not follow any fixed pattern. The residual stresses measured for a low level of diffusible hydrogen (3.916 ml/100 gm) and for a high level of diffusible hydrogen (12.43 ml/100 gm) were almost similar. The maximum transverse and axial stresses were measured at the center of the weld fusion zone. As one move away from the weld center, the magnitude of residual stresses was observed to decrease. In case I, transverse and axial stresses were measured to be 295 MPa and 205 MPa, respectively, while the corrected

transverse and axial stresses were measured and found to be 196 MPa and 102 MPa respectively, as given in Table 17. The maximum value of transverse stress was measured to be 355 MPa for case II, while the maximum axial stress about 218 MPa for case IV. The magnitude of transverse and axial stresses was measured to be in a tensile nature for all the cases. Residual stresses measured 4 mm away from the center of the weld fusion zone were observed to be smaller as compared to stresses measured at the weld center, but the difference of magnitude was very small. The magnitude of residual stresses in the heat affected zone was observed to be similar as measured at 4 mm away from the weld center. In HAZ, the maximum magnitudes of axial stress and transverse stresses were 196 MPa and 231 MPa for case I and case III, respectively. The transverse and axial stresses measured in the root of the welded plate were observed to be compressive in nature. The maximum magnitude was measured for case IV, as shown in Table 17. The corrected axial and transverse stresses were measured using Equations 21 and 22. A significant difference was observed in the ASTM measured value and c the corrected value of residual stresses, as given in Table 17.

3.3. Temperature distribution

The temperature file obtained from the numerical analysis is shown in Fig. 13. It shows the temperature profile for the root pass, 1st pass, 11th pass, 12th pass and final (14th) pass. The temperature profile is represented by the weld fusion zone of the conventional V-groove design, as shown in Fig. 13. The temperature profile for the root pass is predicted at the point of interest in the middle of the root weld, as shown in Fig. 13(a).

Tab. 17. Residual stress results in P92 welded plate

Specimen	Residual stress at weld center, MPa		Residual stress at 4 mm away from center, MPa		Residual stress in HAZ, MPa		Residual stress in root, MPa	
	Axial stress	Transverse stress	Axial stress	Transverse stress	Axial stress	Transverse stress	Axial Stress	Transverse stress
	ASTM/ Corrected value	ASTM/ Corrected value	ASTM/ Corrected value	ASTM/ Corrected value	ASTM/ Corrected value	ASTM/ Corrected value	ASTM/ Corrected value	ASTM/ Corrected value
Case I	205/102	295/196	189/92	170/82	196/97	151/69	-69/-78	-100/-62
Case II	145/61	355/205	164/75	143/67	183/88	145/66	-88/-90	-123/-76
Case III	192/93	305/168	173/81	143/66	154/68	231/124	-137/-123	-116/-65
Case IV	218/110	271/143	196/97	171/82	163/75	149/71	-157/-137	-105/-56

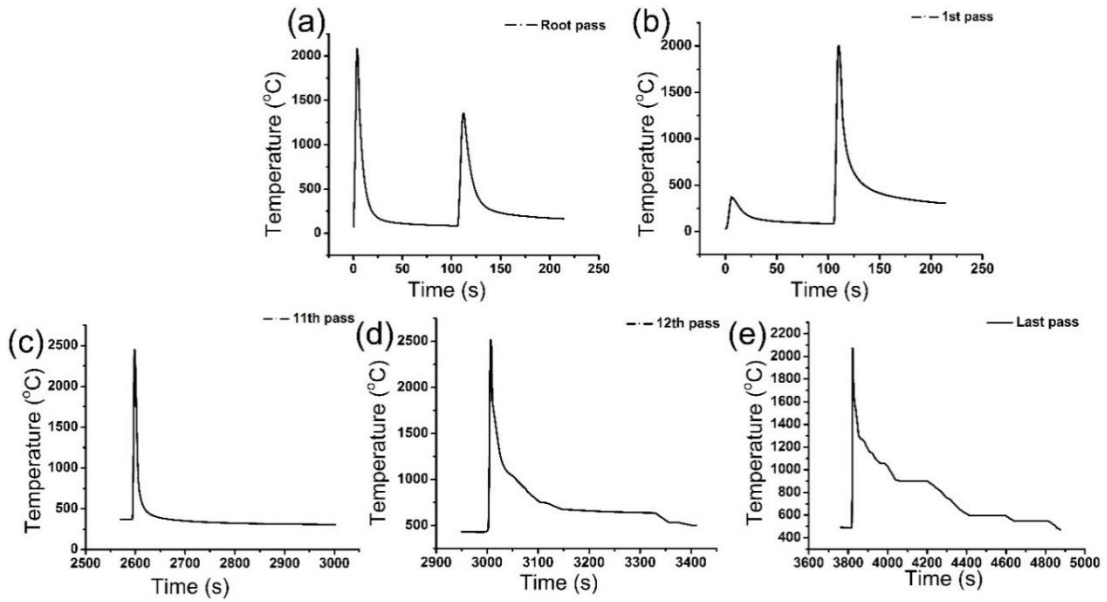


Fig. 13. Predicted temperature distributions of (a) root pass weld, (b) first pass weld and (c) eleventh weld pass, (d) twelfth pass and (e) fourteenth weld pass (last pass)

The temperature profile is shown for the time of 214 seconds. For the root pass, at the center of the weld zone, the peak temperature reaches about 2080°C, which is higher than the melting temperature of P92 steel. The peak temperature falls down below 100°C within 100 seconds. The root pass is further affected by the heat input from the subsequent passes as a result of which the temperature reaches up to 1354°C for the 1st pass in the analysis period of 214 seconds. Fig. 13(b) shows the temperature profile for the point of interest in 1st pass. The 1st pass is affected by the root pass where a preheating effect occurs. The preheating temperature for the 1st pass was calculated to be 360°C. The peak temperature for the 1st pass exceeds 2000°C, as shown in Fig. 13(b). The temperature profiles for the 11th, 12th and the final pass are shown in Fig. 13(c), (d) and (e), respectively. The peak temperature experienced during the 11th, 12th and the final pass was 2440°C, 2485°C, and 2075°C, respectively. From Fig. 13, the peak temperature exceeds the melting temperature of the material during each pass. However, all the points in the weld fusion zone do not reach the same peak temperature.

3.4. Results of structural analysis of conventional V-groove

The numerical simulation was performed for case I. After the structure analysis, the simulated axial and transverse residual stresses were predicted. The distributions of axial and transverse residual stresses are shown in Fig. 14 and 15, respectively. In the weld fusion zone, unsymmetrical distributions of axial and transverse residual stresses are clearly observed. The predicted axial and transverse stresses show a tensile behaviour at the outer surfaces of the welded plate

while a compressive nature of the stresses was observed at the inner surfaces. In the circumferential direction, the range of stress is observed to be lower as compared to the axial direction. The outer surface of the welded plate shows the maximum axial stress at the weld centre. At the inner surfaces (near the weld centre line), the magnitude of residual stresses was observed to be much lower.

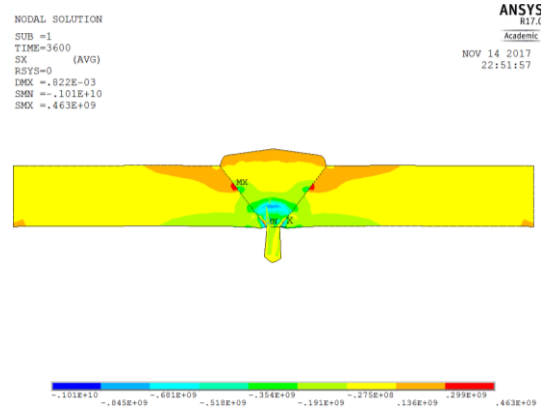


Fig. 14. Simulated axial residual stress distribution for conventional groove

Experimentally measured transverse and axial stresses at the outer surface of the P92 welded plate were compared successfully with the numerically obtained residual stresses value. In Fig. 15, it is observed that the peak axial and transverse residual stresses are obtained near the weld center.

The experimentally measured peak axial and transverse residual stresses were 102 MPa and 196 MPa, as given in Table 17. The lower value of

residual stresses was measured in HAZ, as given in Table 17. The compressive nature of residual stresses was measured in the root section. Based on Fig. 16, the tensile nature of residual stress in the weld zone and HAZ is confirmed, while it measured compressive nature in the root. The predicted residual stresses value matched the numerically obtained residual stresses at the outer surfaces and at the root section. However, some discrepancy is observed between the simulated and experimental results at the weld center for both axial and transverse stresses.

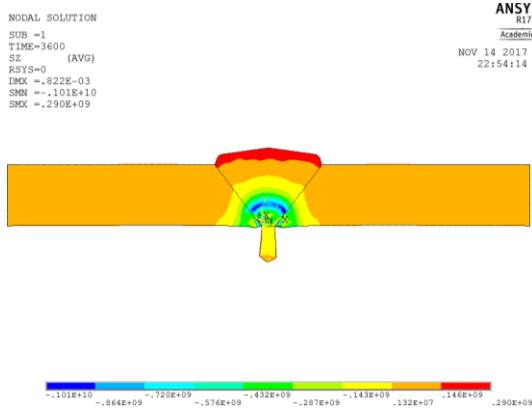


Fig. 15. Simulated transverse residual stress distribution for conventional groove

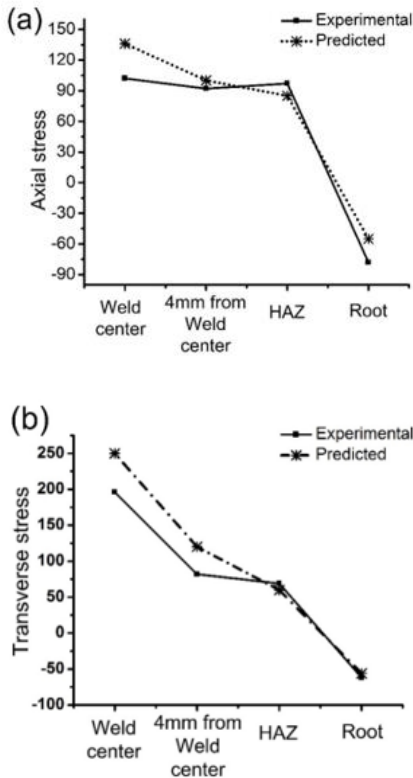


Fig. 16. Numerical and experimental values of residual stresses in P92 welded plate: (a) axial stress and (b) transverse stress

The experimentally measured peak axial and transverse residual stresses were 102 MPa and 196 MPa, as given in Table 17. The lower value of residual stresses was measured in HAZ, as given in Table 17. The compressive nature of residual stresses was measured in the root section. Based on Fig. 16, the tensile nature of residual stress in the weld zone and HAZ is confirmed, while it measured compressive nature in the root. The predicted residual stresses value matched the numerically obtained residual stresses at the outer surfaces and at the root section. However, some discrepancy is observed between the simulated and experimental results at the weld center for both axial and transverse stresses.

4. CONCLUSIONS

1. The transverse shrinkage stress estimated for the V-groove design was approximately 34% of the yield strength of the material, and for the narrow groove it was approximately 23% of the yield strength of the material. Hence, it can be concluded that weld joint is safe against transverse shrinkage stress.
2. The mode and magnitude of transverse shrinkage stresses developed in each quadrant of the pipe is different from each other for the groove design.
3. Transverse shrinkage after each pass increases. Transverse shrinkage that develops in the narrow groove is much smaller than that of the conventional V-groove.
4. The average transverse shrinkage stress was estimated for the conventional V-groove and the narrow groove design of an 11 mm thick P91 pipe. The shrinkage stress estimated for the V-groove and the narrow groove weld designs was 164.33 and 110.33 MPa, respectively.
5. The axial and transverse stresses were measured at the different locations in the centre of the weld fusion zone 4 mm away from the weld fusion zone and HAZ.
6. The maximum magnitude of residual stresses was measured at the centre of the weld fusion zone. The maximum value of transverse stress was 355MPa for case II and 218MPa for case IV, while the maximum axial stresses was measured.
7. The root of the welded plate was observed to be compressive in nature, and transverse and axial stresses were measured. In the numerical value analysis, residual stresses proved to be unsymmetrical in the weld fusion zone.

References

1. M. M. Mahapatra, G. L. Datta, B. Pradhan, and N. R. Mandal, "Modelling the effects of constraints and single axis welding process parameters on angular distortions in one-sided fillet welds," *Proc. IMechE Part B J. Eng.*

- Manuf.*, vol. 221, pp. 397–407, 2006, doi: 10.1243/09544054JMEM617.
2. R. Cottam, V. Luzin, K. Thorogood, Y. C. Wong, and M. Brandt, "The role of metallurgical solid state phase transformations on the formation of residual stress in laser cladding and heating," *Mater. Sci. Forum*, vol. 777, pp. 19–24, 2014, doi: 10.4028/www.scientific.net/MSF.777.19.
 3. A. De and T. Debroy, "A perspective on residual stresses in welding," *Sci. Technol. Weld. Join.*, vol. 16, no. 3, pp. 204–208, 2017, doi: 10.1179/136217111X12978476537783.
 4. P. Biswas, N. R. Mandal, P. Vasu, and S. B. Padasalag, "Analysis of welding distortion due to narrow-gap welding of upper port plug," *Fusion Eng. Des.*, vol. 85, no. 5, pp. 780–788, 2010, doi: 10.1016/j.fusengdes.2010.05.025.
 5. P. Biswas, N. R. Mandal, and S. Das, "Prediction of welding deformations of large stiffened panels using average plastic strain method," *Sci. Technol. Weld. Join.*, vol. 16, no. 3, pp. 227–231, 2011, doi: 10.1179/1362171811Y.0000000004.
 6. P. K. Ghosh, K. Devakumar, and A. K. Pramanick, "Effect of pulse current on shrinkage stress and distortion in multipass GMA welds of different groove sizes," *Weld. J. (Miami, Fla)*, vol. 89, no. 3, pp. 14–23, 2010.
 7. C. Basavaraju, "Simplified analysis of shrinkage in pipe to pipe butt welds," *Nucl. Eng. Des.*, vol. 197, pp. 239–247, 2000.
 8. G. A. Webster and A. N. Ezeilo, "Residual stress distributions and their influence on fatigue lifetimes," *Int. J. Fatigue*, vol. 23, pp. 375–383, 2001.
 9. P. Dong and P. Dong, "Residual stresses and distortions in welded structures: a perspective for engineering applications Residual stresses and distortions in welded structures: a perspective for engineering applications," *Sci. Technol. Weld. Join.*, vol. 10, no. 4, pp. 389–398, 2004, doi: 10.1179/174329305X29465.
 10. P. G. Kumar and K. Yu-ichi, "Diffusible Hydrogen In Steel Weldments," *Trans. JWRI*, vol. 42, no. 1, pp. 39–62, 2013.
 11. A. H. Yaghi, T. H. Hyde, A. A. Becker, and W. Sun, "Finite element simulation of welding and residual stresses in a P91 steel pipe incorporating solid-state phase transformation and post-weld heat treatment," *J. Strain Anal. Eng. Des.*, vol. 43, no. 5, pp. 275–293, 2008, doi: 10.1243/03093247JSA372.
 12. P. Dong, "Residual Stress Analyses of a Multi-Pass Girth Weld: 3-D Special Shell Versus Axisymmetric Models," *J. Press. Vessel Technol.*, vol. 123, pp. 207–213, 2001, doi: 10.1115/1.1359527.
 13. M. Zubairuddin, S. K. Albert, M. Vasudevan, S. Mahadevan, V. Chaudhri, and V. K. Suri, "Thermomechanical analysis of preheat effect on grade P91 steel during GTA welding," *Mater. Manuf. Process.*, vol. 31, no. 3, pp. 366–371, 2016, doi: 10.1080/10426914.2015.1025964.
 14. D. Dean and M. Hidekazu, "Prediction of welding residual stress in multi-pass butt-welded modified 9Cr–1Mo steel pipe considering phase transformation effect," *Comput. Mater. Sci.*, vol. 37, pp. 209–219, 2006, doi: 10.1016/j.commatsci.2005.06.010.
 15. H. Murakawa *et al.*, "Effect of phase transformation onset temperature on residual stress in welded thin steel plates," *Trans. JWRI*, vol. 37, no. 02, pp. 75–80, 2008.
 16. S. Loópez-Ramírez, J. D. J. Barreto, J. Palafox-Ramos, R. D. Morales, and D. Zacharias, "Modeling study of the influence of turbulence inhibitors on the molten steel flow, tracer dispersion, and inclusion trajectories in tundishes," *Metall. Mater. Trans. B*, vol. 32, no. 4, pp. 615–627, 2001, doi: 10.1007/s11663-001-0117-4.
 17. J. M. Cabrera-Marrero, V. Carreno-Galindo, R. D. Morales, and F. Chavez-Alcala, "Macro-Micro modeling of the dendritic microstructure of steel billets processes by continuous casting," *ISIJ Int.*, vol. 38, no. 8, pp. 812–821, 1998.
 18. A. Mitra, N. Siva Prasad, and G. D. Janaki Ram, "Estimation of residual stresses in an 800 mm thick steel submerged arc weldment," *J. Mater. Process. Technol.*, vol. 229, pp. 181–190, 2016, doi: 10.1016/j.jmatprotec.2015.09.007.
 19. A. Mitra, N. Siva Prasad, and G. D. Janaki Ram, "Influence of temperature and time of post-weld heat treatment on stress relief in an 800-mm-thick steel weldment," *J. Mater. Eng. Perform.*, vol. 25, no. 4, pp. 1384–1393, 2016, doi: 10.1007/s11665-016-1995-6.
 20. D. Deng, H. Murakawa, and W. Liang, "Numerical and experimental investigations on welding residual stress in multi-pass butt-welded austenitic stainless steel pipe," *Comput. Mater. Sci.*, vol. 42, no. 2, pp. 234–244, 2008, doi: 10.1016/j.commatsci.2007.07.009.
 21. Y. Sattari-Far, Javadi, "Influence of welding sequence on welding distortions in pipes," *Int. J. Press. Vessel. Pip.*, vol. 85, pp. 265–274, 2008, doi: 10.1016/j.ijpvp.2007.07.003.
 22. S. Kim, J. Kim, and W. Lee, "Numerical prediction and neutron diffraction measurement of the residual stresses for a modified 9Cr – 1Mo steel weld," *J. Mater. Process. Technol.*, vol. 209, pp. 3905–3913, 2009, doi: 10.1016/j.jmatprotec.2008.09.012.
 23. P. K. Ghosh, R. R. Kumar, and A. K. Pramanick, "Effect of pulse current on shrinkage stress and distortion in multi pass GMA welds of different groove sizes," *Indian Weld. Journal Welding J.*, vol. 43-s, pp. 14–24, 2010.
 24. R. Anant and P. K. Ghosh, "Experimental investigation on transverse shrinkage stress and distortion of extra narrow and conventional gap dissimilar butt joint of austenitic stainless steel to low alloy steel," *Proc. Int. Conf. Mining, Mater. Metall. Eng.*, no. 161, pp. 1–5, 2014.
 25. S. Arunkumar, P. Rangarajan, K. Devakumar, and P. Sathiya, "Comparative study on transverse shrinkage, mechanical and metallurgical properties of AA2219 aluminium weld joints prepared by gas tungsten arc and gas metal arc welding processes," *Def. Technol.*, vol. 11, no. 3, pp. 262–268, 2015, doi: 10.1016/j.dt.2015.05.008.
 26. A. H. Yaghi *et al.*, "A comparison between measured and modeled residual stresses in a circumferentially butt-welded P91 steel pipe," *J. Press. Vessel Technol.*, vol. 132, pp. 1–10, 2010, doi: 10.1115/1.4000347.
 27. S. Paddea, J. A. Francis, A. M. Paradowska, P. J. Bouchard, and I. A. Shibli, "Residual stress distributions in a P91 steel-pipe girth weld before and after post weld heat treatment," *Mater. Sci. Eng. A*, vol. 534, pp. 663–672, 2012, doi: 10.1016/j.msea.2011.12.024.
 28. K. A. Venkata, S. Kumar, H. C. Dey, D. J. Smith, and P. J. Bouchard, "Study on the effect of post weld heat treatment parameters on the relaxation of welding residual stresses in electron beam welded P91 steel plates," *Procedia Eng.*, vol. 86, pp. 223–233, 2014, doi: 10.1016/j.proeng.2014.11.032.
 29. T. C. Chuvas, P. S. P. Garcia, J. M. Pardal, and M. da P. C. Fonseca, "Influence of heat treatment in residual stresses generated in P91 steel-pipe weld," *Mater. Res.*, vol. 18, no. 3, pp. 614–621, 2015, doi: 10.1590/1516-1439.006315.
 30. S. Kulkarni, P. K. Ghosh, and S. Ray, "Improvement of weld characteristics by variation in welding processes and parameters in joining of thick wall 304LN stainless steel pipe," *ISIJ Int.*, vol. 48, no. 11, pp. 1560–1569, 2008.
 31. Y. Zhao, J. Gong, Y. Wang, and G. Wei, "Effect of start/stop position distribution on residual stresses in the multi-pass welded 12Cr1MoV/P91 dissimilar pipe," *Int.*

- J. Steel Struct.*, vol. 14, no. 3, pp. 539–546, 2014, doi: 10.1007/s13296-014-3010-0.
32. N. Hempel, T. Nitschke-Pagel, and K. Dilger, “Residual stresses in multi-pass butt-welded ferritic-pearlitic steel pipes,” *Weld. World*, vol. 59, no. 4, pp. 555–563, 2015, doi: 10.1007/s40194-015-0230-7.
 33. M. K. Satyarthi and P. M. Pandey, “Modeling of material removal rate in electric discharge grinding process,” *Int. J. Mach. Tools Manuf.*, vol. 74, pp. 65–73, 2013, doi: 10.1016/j.ijmachtools.2013.07.008.
 34. V. Sharma and P. M. Pandey, “Optimization of machining and vibration parameters for residual stresses minimization in ultrasonic assisted turning of 4340 hardened steel,” *Ultrasonics*, vol. 70, pp. 172–182, 2016, doi: 10.1016/j.ultras.2016.05.001.
 35. R. S. Mulik and P. M. Pandey, “Magnetic abrasive finishing of hardened AISI 52100 steel,” *Int. J. Adv. Manuf. Technol.*, vol. 55, no. 5–8, pp. 501–515, 2011, doi: 10.1007/s00170-010-3102-8.
 36. *ASTM E837-13a, Standard test method for determining residual stresses by the hole drilling strain gage method.* ASTM International, West Conshohocken, PA, 2013, 2013. doi: 10.1520/E0837-13A.2.
 37. M. Z. H. Khandkar, J. A. Khan, A. P. Reynolds, and M. A. Sutton, “Predicting residual thermal stresses in friction stir welded metals,” *J. Mater. Process. Technol.*, vol. 174, no. 1–3, pp. 195–203, 2006, doi: 10.1016/j.jmatprotec.2005.12.013.
 38. L. X. Jang, X. F. Peng, and B. X. Wang, “Numerical modeling and experimental investigation on the characteristics of molten pool during laser treatment,” *Int. J. Heat Mass Transf.*, vol. 44, pp. 4465–4473, 2001.
 39. J. Goldak, “Computer modeling of heat flow in welds,” *Met. Trans.*, pp. 17–26, 1986.
 40. B. Brickstad and B. L. Josefson, “A parametric study of residual stresses in multi-pass butt-welded stainless steel pipes,” *Int. J. Press. Vessel. Pip.*, vol. 75, pp. 11–25, 1998, doi: 10.1016/S0308-0161(97)00117-8.
 41. C. Liu, J. X. Zhang, and C. B. Xue, “Numerical investigation on residual stress distribution and evolution during multipass narrow gap welding of thick-walled stainless steel pipes,” *Fusion Eng. Des.*, vol. 86, no. 4–5, pp. 288–295, 2011, doi: 10.1016/j.fusengdes.2011.01.116.
 42. M. M. Mahapatra, G. L. Datta, B. Pradhan, and N. R. Mandal, “Three-dimensional finite element analysis to predict the effects of SAW process parameters on temperature distribution and angular distortions in single-pass butt joints with top and bottom reinforcements,” *Int. J. Press. Vessel. Pip.*, vol. 83, no. 10, pp. 721–729, 2006, doi: 10.1016/j.ijpvp.2006.07.011.
 43. P. Biswas and N. R. Mandal, “Thermomechanical finite element analysis and experimental investigation of single-pass single-sided submerged arc welding of C-Mn steel plates,” *Proc. Inst. Mech. Eng. Part B J. Eng. Manuf.*, vol. 224, no. 4, pp. 627–639, 2010, doi: 10.1243/09544054JEM1624.
 44. P. Biswas, D. A. Kumar, N. R. Mandal, and M. M. Mahapatra, “A study on the effect of welding sequence in fabrication of large stiffened plate panels,” *J. Mar. Sci. Appl.*, vol. 10, no. 4, pp. 429–436, 2011, doi: 10.1007/s11804-011-1088-8.
 45. TN-503, “Measurement of residual stresses by the hole drilling strain gage method,” *Vishay Precision Group*, pp. 19–33, 2010.

Biographical notes



Vinay Kumar Pal received his M.Tech in Mechanical Engineering (Machine Design) from Faculty of Engineering and Technology, Sam Higginbottom University of Agriculture Technology and Sciences Allahabad in 2017. Currently Ph.D Scholar in Department of Mechanical Engineering, VIAET, Sam

Higginbottom University of Agriculture Technology and Sciences Allahabad. His scientific interests are focused on issues related with Welding, Heat Treatment and Mechanical Behavior of Materials. He has published more than 7 scientific papers in various international and national journals.



Lokendra Pal Singh received his M.E degree in Mechanical Engineering M.L.N.R.E.C Allahabad then next Ph.D in Mechanical Engineering AAIDU Allahabad in 2001 and 2011 respectively. He is working as Associate Professor and Head, Department of Mechanical

Engineering, Sam Higginbottom University of Agriculture Technology and Sciences Allahabad. His scientific interests are focused on issues related with Production and Thermal Engineering. He has published more than 42 scientific papers in various international and national journals as well as conference proceedings.